technologies

Article

Do Nano-Additives Always Improve Electrified Lubrication? Insights from hBN-Containing Grease in Rolling Bearings Under Electrified Conditions

Shubrajit Bhaumik [1,*], Byreddy Lakshmi Manohar Reddy [1], Viorel Paleu [2] and William Woei Fong Chong [3]

[1] Tribology and Interactive Surfaces Research Laboratory (TRISUL), Department of Mechanical Engineering, Amrita School of Engineering, Amrita Vishwa Vidyapeetham, Chennai 601103, India; b.l.manohar6268@gmail.com
[2] Mechanical Engineering, Mechatronics and Robotics Department, "Gheorghe Asachi" Technical University of Iași, 43 Prof. Dimitrie Mangeron Blvd, 700050 Iasi, Romania; viorel.paleu@academic.tuiasi.ro
[3] Automotive Development Centre (ADC), Institute for Sustainable Transport (IST), Universiti Teknologi Malaysia, Johor Bahru 81310, JHR, Malaysia; william@utm.my
* Correspondence: s_bhaumik@ch.amrita.edu

Abstract

The rapid growth of electric vehicles and electrified systems has increased the risk of bearing failures due to combined mechanical and electrical stresses. This study investigated the performance of hexagonal boron nitride nanoparticle-enhanced lithium grease under electrified conditions. Experiments based on a Taguchi L9 orthogonal array were conducted on deep groove ball bearings using a full-scale test rig at 1200 rpm with varying loads (100–300 N), currents (6–10 A), and hBN concentrations (0.1–1 wt.%). The tribo-electrical performance of nano-enhanced grease was compared with the base grease and commercial grease. It was observed that the base grease exhibited superior performance with a lower current flow, reduced vibration, and minimal surface degradation. In contrast, the hBN-enhanced grease exhibited inferior tribo-performance, with high vibrations and surface damage in electrified conditions. The surface analysis revealed features morphologically similar to white etching areas and micro-pitting. The FTIR results indicated grease degradation, while ICP-OES confirmed higher wear debris generation in the commercial and hBN-added greases. The present work indicates that additives like hBN nanoparticles do not necessarily improve performance under electrified conditions, making it important to consider the type of additives to be added during lubricant formulation. Thus, the findings emphasize the importance of lubricant formulation for controlling electrically induced bearing failures and provide insights for developing advanced greases for electric machinery applications.

Keywords: hBN nanoparticles; electrified lubrication; bearing failure; electrical discharge damage; tribology; white etching areas; grease degradation

Check for updates

Academic Editor: Nam-Trung Nguyen

Received: 17 May 2026
Revised: 22 June 2026
Accepted: 23 June 2026
Published: 25 June 2026
Corrected: 23 October 2026

Copyright: © 2026 by the authors. Licensee MDPI, Basel, Switzerland. This article is an open access article distributed under the terms and conditions of the Creative Commons Attribution (CC BY) license.

1. Introduction

The global transition toward electrification, particularly in the automotive and renewable energy sectors, has fundamentally altered the operational demands placed upon critical mechanical components, such as rolling element bearings [1]. In conventional internal combustion engine systems, the bearings primarily experience mechanical and thermal stress, with well-established failure mechanisms and lubrication strategies [2]. However, in electric vehicles (EVs), hybrid systems, and wind turbines, the bearings are

subjected to electrical currents and electrostatic discharges that frequently pass through the bearing assembly [3]. This electrical exposure initiates unique and destructive failure modes that are not adequately addressed by conventional lubricants. These include electrical arcing and spark erosion, which create microscopic craters on bearing surfaces, and fluting, a characteristic washboard-like pattern that accelerates wear and generates excessive noise, vibration, and accelerated degradation of the lubricating grease itself due to localized heating and chemical breakdown [4,5]. These electrically induced failure mechanisms significantly reduce bearing service life, increase maintenance costs, and pose a substantial reliability challenge for the widespread adoption of electrified systems [6]. The emergence of environmentally friendly technologies, including wind turbines and electric vehicles (EVs), has introduced new tribological challenges [7,8]. EVs operate using electric currents that influence the wear and reliability of critical components, including bearings and gears [9]. The unbalanced electromagnetic fields and high-frequency voltage sweeping between the motor's shaft and case cause potential differences between the drives and the drive casing [10]. This difference in potential causes the current to flow by the bearing race and ball bearings to the gear case, resulting in electrically induced bearing damage (EIBD) [11]. Several insulation strategies, including ceramic bearings, insulating coatings, carbon brushes, and conductive greases, have been employed to mitigate electrically induced bearing damage [12]. In addition, electrical properties of lubricants, specifically greases, are of significant importance in the performance of lubricants in an electrified environment [13]. Electrical discharge damages may occur, attributable to the dielectric nature of lubricants at great lengths. Some recent works have aimed to quantify the breakdown voltage and impedance of lubricated contacts, and the use of specialized lubricants to counter electrical wear has emerged as a possibility [14–19]. It has also been documented that the addition of conductive nanoparticles changes the electrical resistivity and thermal conductivity of greases, and this might help in minimizing the electrical discharges experienced [20].

Improving the understanding of lubricant behavior under electrified operating conditions can help mitigate wear and enhance system reliability through effective control of electrical conductivity [21]. Other studies have also focused on the synthesis of nanoparticles, such as Mn-Zn-Fe, as a solution for tribology magnets in magnetic fields [22,23]. As was recently shown, DC currents influence the film thickness of oil films and lubricant behavior, making it clear that electrical conditions influence tribological performance [24]. Hexagonal boron nitride (hBN) is a promising solid lubricant additive for EV greases because of its unique tribological properties [25]. The key challenges include the high rotational speeds, elevated thermal loads from the motor and battery systems, and electrical current leakage across bearing contacts [26]. hBN is structurally referred to as white graphite, which is another member of a layered crystal with strong covalent bonding between both boron and nitrogen atoms stacked using weak van der Waals forces that enable the shearing and sliding of nanosheets of this material with ease [27,28]. This feature provides hBN with a very low friction rate and enhanced wear minimization. As nanoparticles in grease formulations, when dispersed, permeate the microscopic contact points between the rolling elements and races, creating a physically separated, self-healing tribo-film that suppresses the effects of abrasive and adhesive wear and thus extend the service life of high-value, high-speed motor bearings is of great importance. Further, these particles could serve as nanoscale spacers, which would provide a ball-bearing effect and a decrease in rolling resistance and frictional losses [29].

In addition to its mechanical advantages, the electrical and thermal properties of hBN are particularly relevant for electric vehicle applications. Unlike conventional solid lubricants, such as graphite or metallic particles, hBN is a wide-bandgap electrical insulator

with high dielectric strength. These properties enable hBN to impede stray current flow and reduce the likelihood of electrical discharge machining (EDM)-related damage in bearing systems. Electrical discharges can produce micro-arcing, localized melting, surface erosion, pitting, noise, and premature bearing failure [30–33]. By interrupting the conductive pathways, hBN may enhance the electrical insulation of lubricated contacts and contribute to improved reliability of electric motor bearings. In addition, hBN nanoparticles possess high thermal conductivity, which is beneficial in managing the frictional heat generated by high-speed rolling bearings and the heat originating from adjacent motor and battery systems [34]. Its ability to facilitate efficient heat dissipation helps maintain lubricant stability, minimize localized temperature rise, and reduce thermally induced wear. Consequently, hBN nanoparticles have the potential to improve both the thermal management and operational durability of bearing systems operating under electrified conditions.

Electric field-induced bearing failures of several types exist. Electrical discharge damage or electric erosion is a widespread condition in electrified mechanical components. This causes several types of damage, which include local heat, aggravation of noise and vibration, lubricant degradation and, ultimately, premature bearing failure [35]. These currents arise from several factors, including uncontrolled electromagnetic fields and high-frequency inverter switching voltages [20]. They are capable of leaving characteristic patterns of damage, which are frosting, fluting, and pitting. Despite the recognized potential of nano-enhanced lubricants, a critical knowledge gap exists in the literature regarding their performance under the combined influence of mechanical loading and electrical current in realistic bearing geometries [36]. Most existing studies rely on simplified tribometers, such as pin-on-disk or four-ball testers, which do not replicate the complex contact mechanics, kinematics, and dynamic environment of an actual rolling element bearing. Furthermore, systematic investigations that explore the synergistic effects of multiple operating parameters, such as current magnitude, applied load, and additive concentration, on both the mechanical wear and electrical degradation remain scarce [37]. This research addresses these gaps by experimentally investigating the failure mechanisms of deep groove ball bearings lubricated with hBN-enhanced lithium grease under electrified conditions. Using a Taguchi L9 orthogonal array experimental design, this study systematically evaluates the effects of current, load, and hBN concentration on the bearing performance, comparing the optimized formulation with baseline and commercial greases. The findings aim to provide empirical data on the efficacy of hBN as a multi-functional additive, contributing to the development of advanced lubricants that can enhance the reliability and longevity of bearings in electric and hybrid systems.

2. Materials and Methods

2.1. Materials

Mineral oil (used as the base oil) was purchased from a local oil supplier in Chennai, India. The physicochemical properties of mineral oil are shown in Table 1.

Table 1. Physicochemical properties of mineral oil.

Parameters	Unit	Value
Viscosity at 40 °C	cSt	584.2
Viscosity at 80 °C	cSt	21
Flash Point	°C	250
Fire Point	°C	280
Total Acid Number (TAN)	MgKOH/g	0.62
Sulfur Content	ppm	5076

The base oil was used without any further purification. Hexagonal boron nitride nanoparticles (hBN nanoparticles) (Make: Nanoshel; Chennai, India) average particle size, 60 nm; CAS No. 10043-11-5) were used as additives in the lithium grease.

2.2. Preparation of the Grease Samples

In this work, hBN nanoparticles were added, as a weight percentage (wt. %), to 12-hydroxy lithium stearate, with mineral oil as the base oil. High-shear mechanical mixing and three-mill grinding ensured uniform distribution of hexagonal boron nitride (hBN) nanoparticles within the base grease matrix. Three grease formulations containing hBN concentrations of 0.1 wt.%, 0.5 wt.%, and 1.0 wt.% were then evaluated. In addition to the hBN-containing greases, a control base grease (BG) without hBN nanoparticles was also synthesized following an identical preparation procedure, including sonication, heating, homogenization, and three-mill grinding. This was done to isolate the effects of hBN addition on the tribological and electrical performance.

Cheng et al. [38] indicated that grease with 1 wt.% hBN nanoparticles can reduce wear by 20%; hence, the hBN nanoparticle concentration was restricted to 1 wt.%. Initially, the hBN nanoparticles were added to the mineral oil and sonicated intermittently for 30 min using a probe sonicator (Make: Athena, Navi Mumbai, India; Model: 4.3 TFT) to ensure uniform dispersion. This dispersion was then mixed with 17 g of 12-hydroxy lithium stearate thickener. In order to produce a homogeneous mixture, the oil–thickener mixture was thoroughly mixed using a mechanical stirrer for 30 min. The mixture was then gradually heated to 220 °C and maintained at 220 °C for 20 min. Continuous stirring was done to ensure uniform heat distribution. The mixture was then cooled down to room temperature, thus obtaining the coarse grease. It was further refined and homogenized by passing it through a horizontal roller at an applied load of 50 N. The coarse grease was ground for 5 h, ultimately resulting in a fine grease structure. Figure 1 shows the schematic diagram of the grease formulation process. Figure 2 shows the prepared grease and the commercial lithium grease (CG), base grease (BG), and grease containing hBN nanoparticles (hBN grease). Table 2 shows the physicochemical properties of the greases.

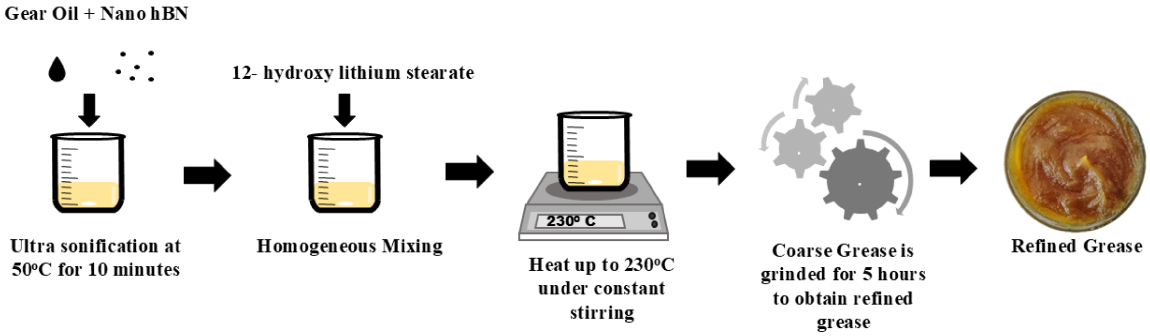

Figure 1. Process of grease synthesis.

Table 2. Physicochemical properties of greases.

Test Parameter	Unit	CG	BG	0.1 wt.% hBN Grease	0.5 wt.% hBN Grease	1.0 wt.% hBN Grease
Unworked Penetration	mm	272 ± 3	340 ± 3	334 ± 2	336 ± 2	336 ± 3
Worked Penetration, 60 Double Strokes	mm	266 ± 2	355 ± 2	329 ± 3	329 ± 3	330 ± 2
Drop Point	°C	180 ± 2	170 ± 2	180 ± 2	182 ± 2	182 ± 2

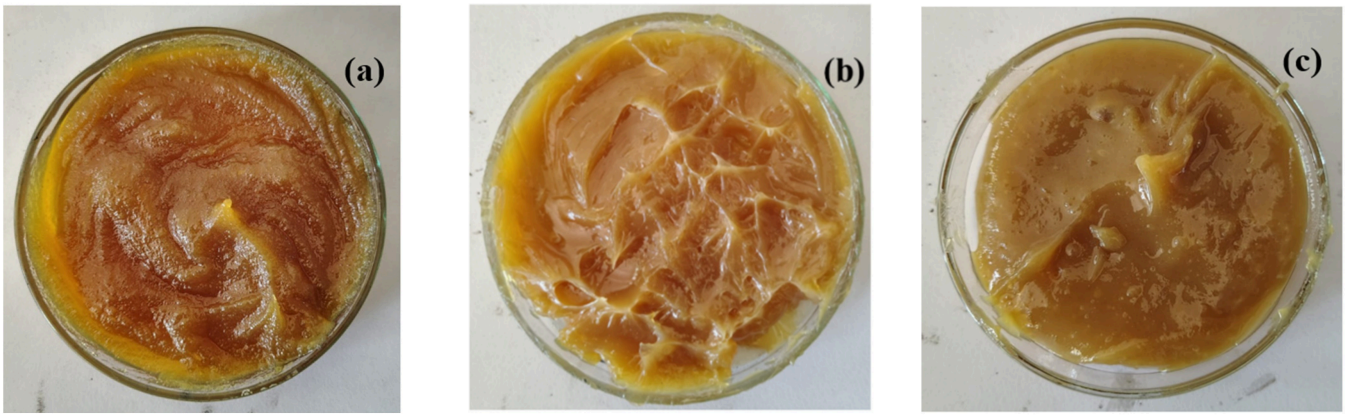

Figure 2. Pictographs of (**a**) BG, (**b**) CG, and (**c**) hBN grease.

A commercial motor bearing grease of type NLGI 2 (procured from Max Grease Agency, Chennai, India) was chosen as a benchmark against which to evaluate the prepared grease. An elemental analysis of the greases was performed using ICP-OES (Make: Perkin Elmer (Shelton, CT, USA); Model: AVIO 220 Max) as per ASTM D 5185 (Table 3). The ICP-OES analysis revealed the presence of zinc, phosphorus, sulfur, calcium, magnesium, and lithium in all grease formulations (Table 3). The commercial grease (CG) exhibited comparatively higher concentrations of calcium and lithium, while the formulated greases contained substantially higher boron concentrations due to the incorporation of hBN nanoparticles. Although phosphorus-, sulfur-, zinc-, and calcium-containing species were detected in both the commercial and formulated greases, significant differences existed in their elemental concentrations and overall additive chemistries. The formulated hBN greases were developed primarily to investigate the influence of hBN nanoparticles under electrified conditions. In contrast, the commercial grease represents a proprietary EV grease formulation containing a different additive package. Therefore, the comparison with the commercial grease should be interpreted as a benchmark comparison of tribological and electrical performance rather than a direct one-to-one comparison of equivalent additive chemistries. Table 4 presents the Taguchi L9 orthogonal array design for the experiments. Three critical factors were selected for investigation of electrical current at three levels (6 A, 8 A, and 10 A) and applied mechanical load at three levels (100 N, 200 N, and 300 N). The experimental design, combined with the systematic preparation protocol, provided a comprehensive and efficient framework for investigating the synergistic effects of electrical current, mechanical load, and additive concentration on bearing failure mechanisms in electrified environments.

Table 3. Elemental analysis of greases.

Elements	Unit	CG	BG	0.1 wt% hBN Grease	0.5 wt% hBN Grease	1.0 wt% hBN Grease
Boron	ppm	40	12	5881	12,220	19,986
Magnesium	ppm	33	7	9	11	9
Zinc	ppm	156	106	128	131	131
Phosphorus	ppm	334	357	210	214	211
Calcium	ppm	501	137	139	148	152
Molybdenum	ppm	5	6	8	8	8
Sulfur	ppm	4975	5116	8611	8591	8626
Lithium	ppm	3224	1422	1329	1239	1291

Table 4. L9 array detailing test conditions for each experimental run.

Experiment	Current (A)	Load (N)	hBN (wt%)
E1	6	100	0.1
E2	6	200	0.5
E3	6	300	1
E4	8	100	0.5
E5	8	200	1
E6	8	300	0.1
E7	10	100	1
E8	10	200	0.1
E9	10	300	0.5

2.3. Determining the Bearing Failures Using a Roller Bearing Test Rig Under an Alternating Current

Figure 3 shows the experimental setup (Make: Magnum Engineers; Bangalore, India) used in this work [39]. Deep groove ball bearings (SKF 6206) were used as the test bearings in this study. Table 5 exhibits the bearing component steel composition, determined as per JIS G1253-13 standards [40]. About 5.0 ± 0.5 g of grease (calculated based on the standard grease-fill formula) was introduced into the bearings. Uniform grease distribution was promoted by manually rotating the bearings after grease filling to facilitate grease coverage of the rolling elements and raceways; however, no independent quantitative verification of grease distribution was performed. The experiments were carried out by passing alternating electric currents (6 A, 8 A, and 10 A) through the test bearing fitted on the shaft. The bearings were rotated at 1200 rpm under radial loads of 100 N, 200 N, and 300 N. Each test was conducted for 12 h. The test rig was connected to a 220 V, 50 Hz power supply. The test rig was surrounded by an insulator (Hylem) to avoid any accidental electric current passage outside the test rig. The radial vibrations due to the surface damage of the bearing raceways were picked up by an accelerometer (Make: PCB; Model: 333B30, Depew, NY, USA) attached to the top of the bearing housing. Each set of experiments was repeated twice. The current, voltage, and vibration signals were continuously recorded throughout the 12 h test duration using the data acquisition system integrated within the test rig. The reported average current, voltage, and vibration values correspond to the arithmetic mean values calculated over the complete 12 h test duration, encompassing both the transient running-in period and the quasi-steady-state operating regime. The final reported values represent the mean of two independent experimental runs conducted under identical operating conditions. No external temperature control system was employed during the experiments, and all tests were conducted under laboratory ambient conditions (37.5 ± 0.7 °C).

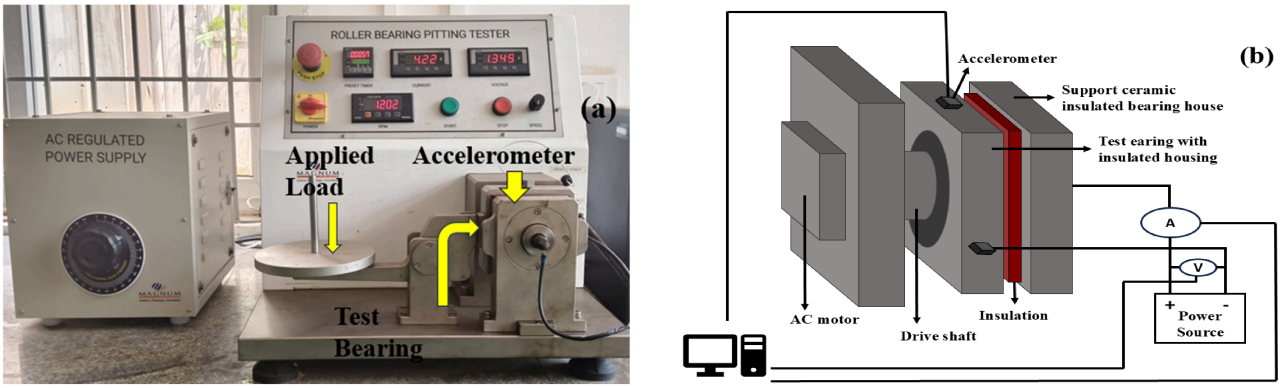

Figure 3. (**a**) Bearing test rig; (**b**) schematic diagram of the bearing test rig.

Table 5. Composition of the bearing parts.

Bearing Parts	Carbon (%wt.)	Manganese (%wt.)	Silicon (%wt.)	Sulfur (%wt.)	Phosphorus (%wt.)	Chromium (%wt.)
Raceway	0.934	0.381	0.234	0.011	0.005	1.421
Bearing balls	0.916	0.350	0.240	0.017	0.022	1.370
Cage	0.064	0.233	-	0.014	0.017	-

2.4. Surface Characterization of the Bearing Raceways to Determine the Wear Patterns

An optical microscope (Make: Olympus, Model BX53M, Bengaluru, India) was used to inspect the bearing raceways for damage under magnification of 10×.

2.5. Hardness Measurement of the Bearing Raceways

Rockwell hardness measurements were performed on the bearing raceways after testing. Five measurements were taken at different locations along the damaged raceway surface, and the reported hardness value represents the arithmetic mean of these measurements. A Rockwell C scale with a 150 kgf major load was employed. Care was taken to avoid overlapping indentations and severely damaged regions.

2.6. Analysis of Greases to Determine Their Degradation

To assess the severity of wear, the iron contents of the greases after the test were evaluated using Inductively Coupled Plasma Optical Emission Spectroscopy (ICP-OES) (Make: Perkin Elmer (USA); AVIO 220 Max). Following the test, approximately 1 mg of each grease was collected and utilized to determine the iron concentration using ICP-OES. The ICP-OES experiments were carried out using the ASTM D5185 method [41,42]. About 0.3 g of grease was placed in a tube and diluted with 10 mL of white mineral oil. The mixture was properly combined to dissolve the grease. After calibrating the equipment and determining the iron wavelength, the diluted liquid was examined using ICP-OES. The grease degradation was further examined using Fourier transform infrared spectroscopy (FTIR) (Make: Bruker (Billerica, MA, USA); Model: Alpha). The FTIR (attenuated total reflectance (ATR)) analysis was primarily employed as a qualitative tool to compare the spectral changes before and after testing under electrified conditions. The FTIR spectra were converted and presented in absorbance form for qualitative comparison of spectral variations obtained using the ATR mode. A thin layer of test grease was applied to the attenuated total reflectance (ATR) crystal to ensure there were no entrapped bubbles. As a reference sample, approximately 1 mg of fresh grease was deposited on the platinum ATR crystal. A spectrum was generated for this new grease, which became the base grease spectrum. The differences in spectral features between the fresh and tested greases were used as a qualitative indicator of chemical alteration and lubricant degradation.

3. Results and Discussion

3.1. Performance of the Greases Under Electric Current

Figure 4 presents a comparative analysis of average current, voltage, and vibration recorded during the tribological tests conducted using the Taguchi L9 experimental design. As shown in Figure 4a, the average current varied significantly across the nine experimental runs, ranging from 3.6 A to 8.4 A. The lowest average current (3.6 A) was observed in Experiment 2 (E2), corresponding to test conditions of 6 A applied current, 100 N load, and 0.5 wt.% hBN concentration. In contrast, the highest average current (8.4 A) was recorded in Experiment 8 (E8), which involved a 10 A applied current, 200 N load, and 0.1 wt.% hBN nanoparticle concentration. The base grease (BG) exhibited an average current of 4.6 A,

while the hBN grease showed a slightly higher value of 5.3 A. The commercial grease (CG) demonstrated the highest average current among the reference samples, at 5.6 A. These results indicate that the BG offered a relatively higher resistance to electrical current flow under the given test conditions, whereas the addition of hBN nanoparticles and the use of commercial grease tended to increase current conduction.

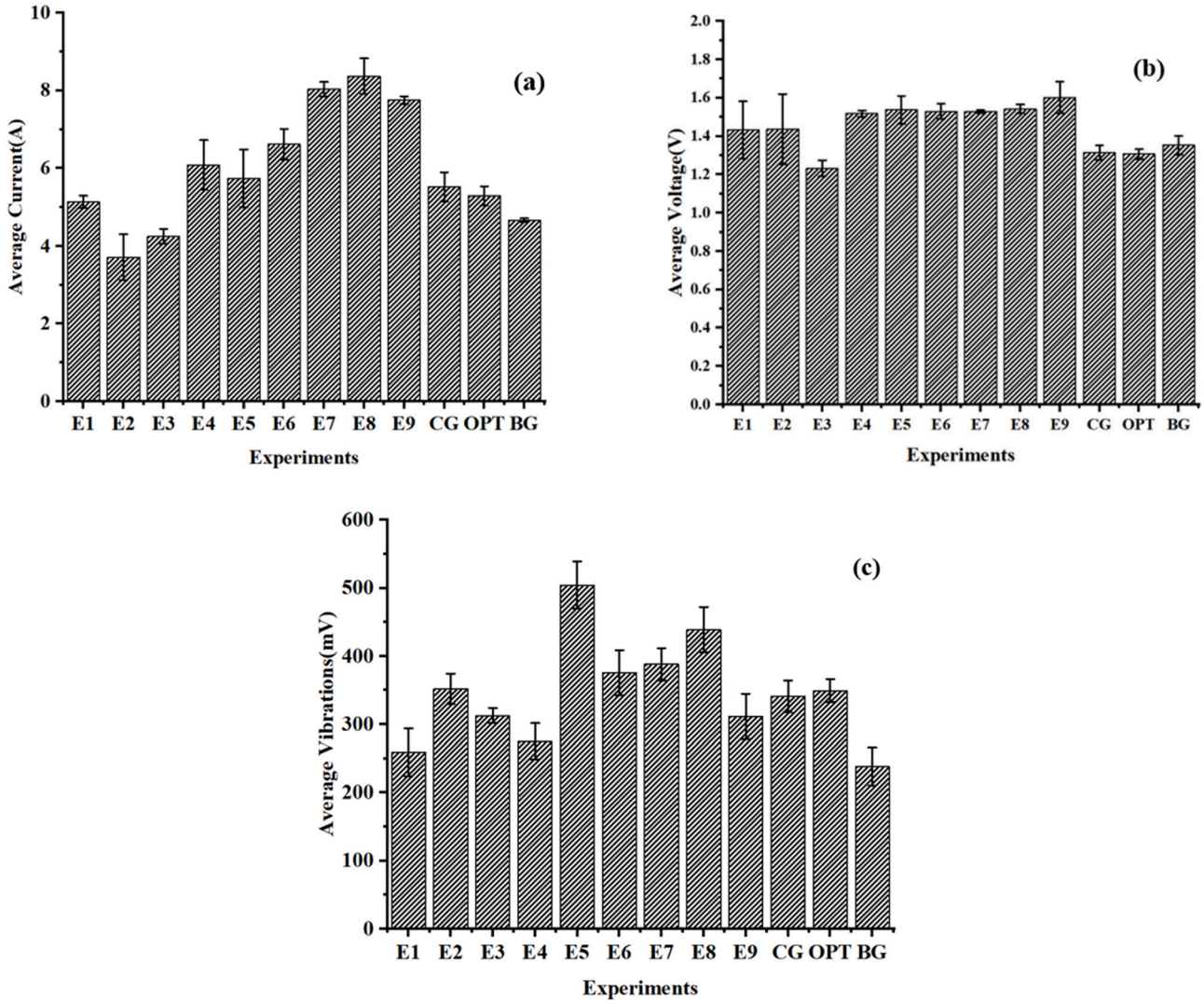

Figure 4. Comparison of average current, voltage, and vibration values obtained from the complete 12 h test duration for the Taguchi L9 experiments and reference grease formulations: (**a**) average current, (**b**) average voltage, (**c**) average vibrations.

The average voltage results presented in Figure 4b indicate that Experiment 9 (E9) recorded the highest average voltage of 1.64 V, corresponding to test conditions of 10 A applied current, 300 N load, and 0.5 wt.% hBN concentration. In contrast, Experiment 3 (E3) exhibited the lowest average voltage of 1.24 V under conditions of 6 A applied current, 300 N load, and 1.0 wt.% hBN concentration. With respect to vibration (Figure 4c), the highest average vibration of 532 mV was observed for Experiment 8 (E8), conducted at 10 A applied current, 200 N load, and 0.1 wt.% hBN concentration. The BG exhibited a significantly lower average vibration of 238.2 $\pm$ 27.83 mV, while the commercial grease was recorded at 337.79 $\pm$ 1.27 mV. This corresponds to an approximately 60% reduction in vibration for the base grease compared to the commercial grease, suggesting superior lubrication stability and more effective film formation. Although some hBN-containing formulations exhibited lower vibrations than other hBN formulations, the base grease

demonstrated the lowest overall vibration response. However, detailed insights into the lubrication mechanisms require analysis of transient behavior. This is particularly important because the bearing–grease system exhibited a prolonged running-in period before reaching quasi-steady-state conditions. The optimum condition (OPT) is discussed in Section 3.2.

3.2. Statistical Analysis of the Experimental Results

Based on the Taguchi optimization method, the optimum condition, considering the experimental conditions shown in Table 4, was identified as 0.5 wt.% hBN nanoparticles at an applied current of 6 A and a load of 100 N (Supplementary Materials). The OPT values shown in Figure 4 correspond to this optimized condition (0.5 wt.% hBN, 6 A, 100 N). However, under these optimized conditions, the grease containing 0.5 wt.% hBN nanoparticles (hBN grease) exhibited higher bearing vibration levels compared to both the BG and CG. This indicates that the incorporation of hBN nanoparticles did not enhance the tribological performance under electrified conditions and, instead, resulted in inferior performance relative to the base grease and commercial grease. Figure 5 illustrates the instantaneous time-series evolution of current, voltage, and vibration during the 12 h tribological tests for the representative BG, CG, and hBN grease samples. As shown in Figure 5a, the applied current was initially set at 6 A and gradually decreased before stabilizing. The steady-state current values were approximately 4.8 A for the commercial grease, 4.4 A for the base grease, and 4.5 A for the hBN grease after 43,200 s. Fluctuations in current were observed throughout the test duration due to the heterogeneous nature of grease, which consists of base oil, thickener, and additives. The base oil acts as an insulating medium, and current conduction occurs when the voltage across the asperity contacts exceeds the dielectric strength of the lubricant film. Since the asperity gap varies dynamically during sliding, intermittent electrical contact results in current fluctuations. The vibration values shown in Figure 5 correspond to the instantaneous time-series responses under specific electrified and non-electrified conditions, whereas Figure 4 presents the average vibration values calculated over the complete 12 h test duration. Therefore, the numerical values in Figures 4 and 5 are not directly comparable. The slight difference between the average current values reported in Figure 4 and the steady-state values shown in Figure 5a arises because Figure 4 reports the arithmetic mean over the entire test duration, including the transient running-in period, whereas Figure 5a highlights the stabilized current response at later stages of operation.

Figure 5b presents the voltage evolution over time. Initially, the base grease exhibited the highest voltage (~1.22–1.25 V), while the commercial grease showed the lowest (~1.05–1.10 V). Over time, all the samples converged and stabilized within the range of ~1.25–1.35 V. Notably, the hBN grease achieved the highest steady-state voltage (~1.40–1.45 V around 21,600 s), indicating enhanced electrical resistance and improved insulating behavior compared to the other greases. The voltage values shown in Figure 5b correspond to the stabilized instantaneous responses and therefore may differ from the average values reported in Figure 4b, which include both the transient and steady-state periods.

Figure 5c shows the variation in the vibration amplitude with time under both current and no-current (NOC) conditions. At the initial stage (0–3000 s), all samples exhibited similar vibration levels (~140–170 mV), indicating stable initial contact conditions. Under an electrical current, the hBN grease showed a rapid increase in vibration to ~400–420 mV by 7200 s, followed by stabilization. The commercial grease exhibited greater instability, with the vibration increasing progressively and reaching peaks of ~480–520 mV after 30,000 s, indicating lubrication degradation.

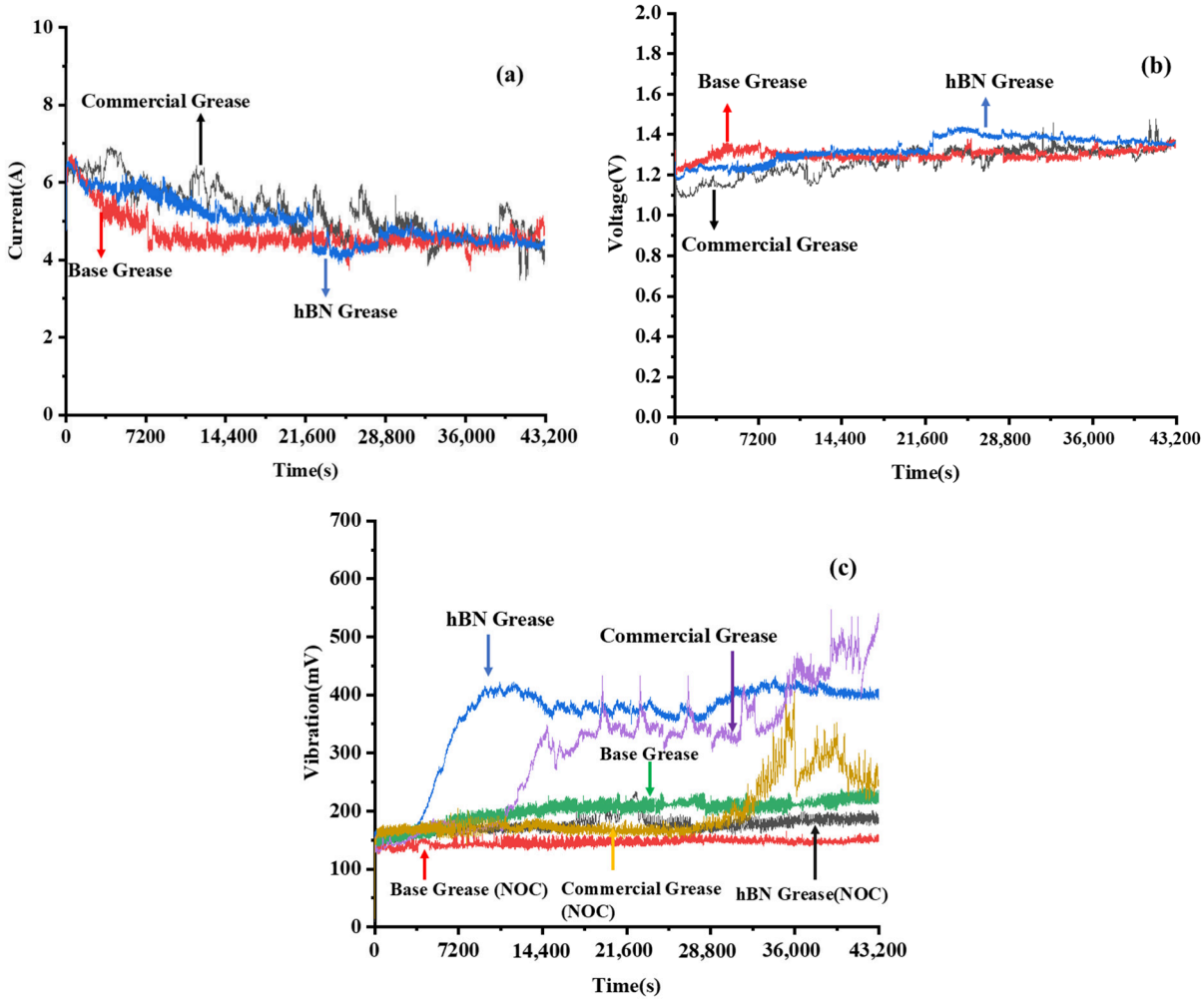

Figure 5. Time-series graph of greases: (**a**) current; (**b**) voltage; (**c**) vibration.

Under the no-current conditions (NOC), all the greases exhibited significantly lower vibration levels. The BG maintained the lowest and most stable average vibration (~140–160 mV), followed by the hBN grease (~160–180 mV), while the CG showed late-stage instability with increasing vibration (~250–320 mV).

The elevated vibration under electrified conditions can be attributed to electrical discharge events, lubricant film breakdown, and increased asperity interactions, leading to higher friction and surface damage. Overall, the results confirm that electrical current adversely affected tribological stability, particularly for the CG, whereas the BG exhibited superior performance and stability under both electrified and non-electrified conditions.

It is important to note that the current traces exhibited a prolonged transient period before reaching quasi-steady-state conditions. As shown in Figure 5a, stabilization of the current occurred after approximately 18,000–20,000 s of operation. This behavior is attributed to the running-in process of the bearing–lubricant system, during which the grease underwent redistribution within the raceway contacts, the asperity interactions evolved, and the electrical contact conditions progressively stabilized. Consequently, a significant portion of the test duration was characterized by transient tribo-electrical behavior rather than fully developed steady-state conditions. However, this transient response is considered representative of practical bearing operation under electrified conditions, where lubricant film formation, electrical discharge activity, and surface adaptation continuously evolve during service. The average current, voltage, and vibration values reported in this

study therefore represent the overall tribo-electrical behavior throughout the complete test duration, encompassing both the transient and quasi-steady-state regimes.

An ANOVA analysis was performed using the vibration responses obtained from all nine Taguchi L9 experimental runs using the varying hBN concentrations (0.1–1 wt.%), applied currents, and loads listed in Table 4. The ANOVA helped in determining the most influential factor as well as specifying the percentage (%) of contribution [39]. Table 6 lists the ANOVA results for vibration versus current, load, and % hBN. The ANOVA was conducted with a significance level of 0.95, which is equivalent to a 95% confidence level for investigation. The statistical analysis indicates that the applied load had the most significant influence on vibration behavior, contributing 51.5% to the overall response with a *p*-value of 0.049, which is below the significance threshold of 0.05. This demonstrates that mechanical loading plays a dominant role in governing vibration and tribological instability in electrified bearing systems. In comparison, the contributions of hBN nanoparticle concentration and applied current were found to be 23.6% and 22.1%, respectively. Although both parameters showed a noticeable influence on the vibration response, their *p*-values were greater than 0.05, indicating that their individual effects were not statistically significant within the investigated range of conditions. The model summary further demonstrates good agreement between the experimental and predicted data, with a regression square (R^2) value of 97.34% and an adjusted R^2 value of 89.37%, indicating that the developed model adequately explains the variability in the experimental results. However, the predicted R^2 value of 46.18% suggests moderate predictive capability, which may be attributed to the complex interaction among the electrical discharge phenomena, lubricant degradation, and surface damage mechanisms occurring during electrified operation. The low error contribution of 2.8% confirms the reliability and consistency of the experimental observations. Thus, the ANOVA results indicate that the applied load is the governing factor affecting vibration characteristics under electrified lubrication conditions, while the hBN concentration and current exhibit secondary influences.

Table 6. ANOVA table for vibration versus current, load and %hBN.

Parameters	Degree of Freedom	Adjusted Sum of Squares	Adjusted Mean of Squares	F-Value	*p*-Value	% Contribution
Current	2	11,071	5535.7	8.32	0.107	22.1
Load	2	25,816	12,908.1	19.39	0.049	51.5
% hBN	2	11,860	5930.2	8.91	0.101	23.6
Error	2	1331	665.5			2.8
Total	8	50,079				100
Model Summary	S	R^2	R^2_{adj}	R^2_{pred}		
	25.7981	97.34%	89.37%	46.18%		

3.3. Determining the Degradation of Grease During the Tribo-Test

Figure 6 indicates that lubricant deterioration occurred within the bearing system during testing and may have contributed to the observed reduction in electrical resistance. This degradation was initially evidenced by the visible discoloration of grease samples, serving as a qualitative indicator of chemical breakdown. Under the influence of electrical current, the grease samples exhibited more pronounced discoloration, suggesting that electrical exposure may accelerate lubricant deterioration. Further insight into lubricant degradation was obtained using an ATR-FTIR analysis. The observed discoloration of the grease samples after testing suggests that chemical changes occurred during tribological operation, particularly under electrified conditions. Previous studies have reported that electrically stressed lubricants may undergo chemical alteration through mechanisms

involving localized heating, lubricant film breakdown, oxidation, and electrochemical reactions at the contact interface [43–50]. However, the present ATR-FTIR analysis was primarily intended to provide qualitative evidence of chemical changes occurring within the grease formulations rather than direct identification of specific degradation pathways. Therefore, the following discussion focuses on the relative spectral changes observed before and after testing.

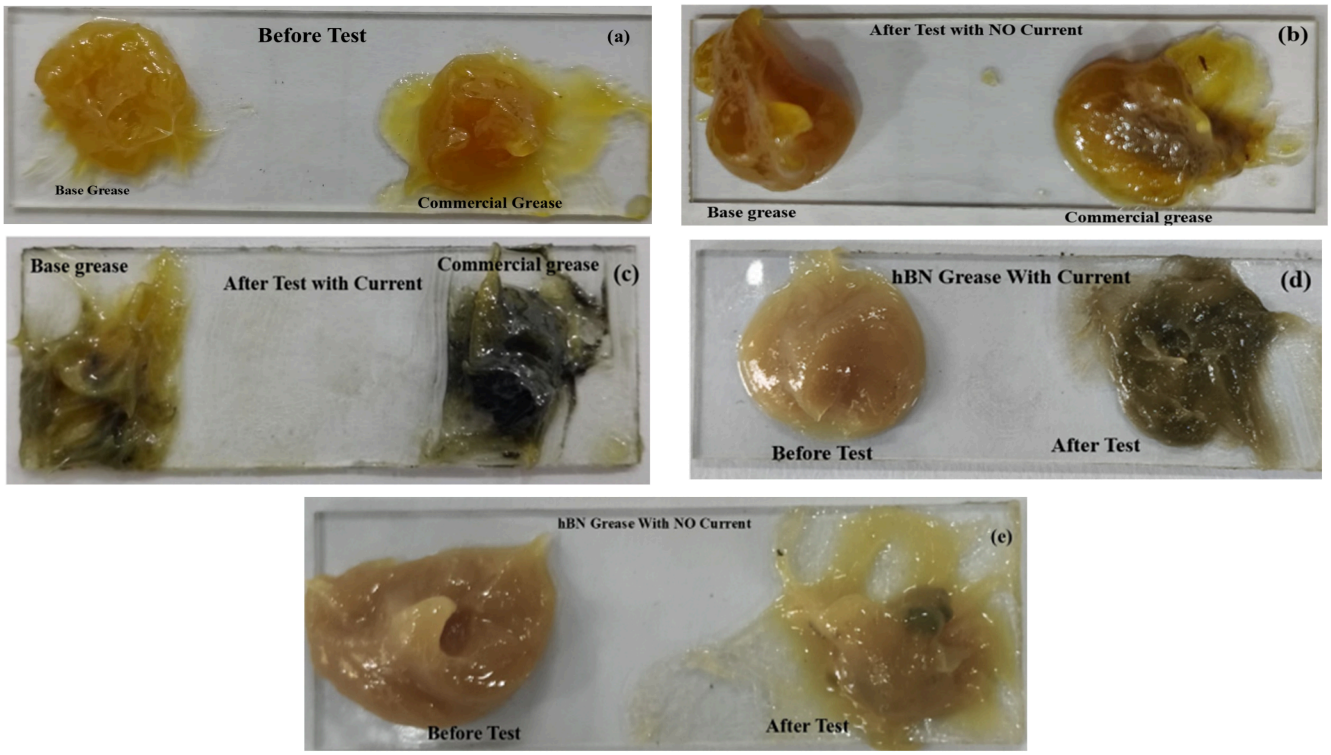

Figure 6. Discoloration of grease after tests with current and no current for (**a**) BG and CG before test, (**b**) BG and CG with no current, (**c**) BG and CG after test with current, (**d**) hBN grease after test with current, and (**e**) hBN grease after test with no current.

The degradation behavior of the greases under non-electrified conditions was further evaluated using the difference ATR-FTIR spectra obtained by subtracting the spectrum of the fresh grease from that of the grease after tribological testing (Figure 7). The use of difference spectra enhanced the visibility of subtle spectral changes that were not readily distinguishable in the original spectra. In the difference spectra, positive bands indicate an increase in absorbance relative to the fresh grease spectrum, whereas negative bands indicate a decrease in absorbance. These changes may be associated with the formation, transformation, or depletion of chemical species during tribological testing.

For the base grease (Figure 7a), only minor spectral deviations were observed across the investigated wavenumber range, indicating limited chemical alteration during the tribological test. In contrast, the commercial grease (Figure 7b) exhibited more pronounced spectral variations, particularly within the oxidation-sensitive regions of 1800–1660 cm^{-1} and 1300–1000 cm^{-1}. Weak spectral features were observed in these regions, which are commonly associated with carbonyl-containing and oxygen-containing degradation products formed during lubricant oxidation. The weak positive features observed in the region of 1800–1660 cm^{-1} may be attributed to the formation of carbonyl-containing oxidation products, including aldehydes, ketones, carboxylic acids, esters, and related oxygenated species, formed during lubricant degradation. The minor spectral changes observed in the 1300–1000 cm^{-1} region may correspond to C–O-containing oxygenated species generated

during oxidation reactions, including alcohols, ethers, peroxides, and ester-type oxidation products. However, the low intensity of these bands and the qualitative nature of the ATR-FTIR measurements prevent a definitive assignment of specific peroxide, alcohol, ester, or carboxylate structures. The relatively low intensity of these bands further suggests that oxidation, if present, remained limited under the test conditions investigated. The hBN grease (Figure 7c) exhibited intermediate behavior, showing greater spectral variation than the base grease but less pronounced changes than the commercial grease. Overall, the difference spectra indicate that the base grease underwent the least chemical alteration during tribological testing, whereas the commercial grease exhibited a comparatively greater degree of chemical alteration. The ATR-FTIR results therefore provide qualitative evidence of degradation-related chemical changes, but should not be interpreted as definitive proof of extensive oxidation or specific degradation pathways.

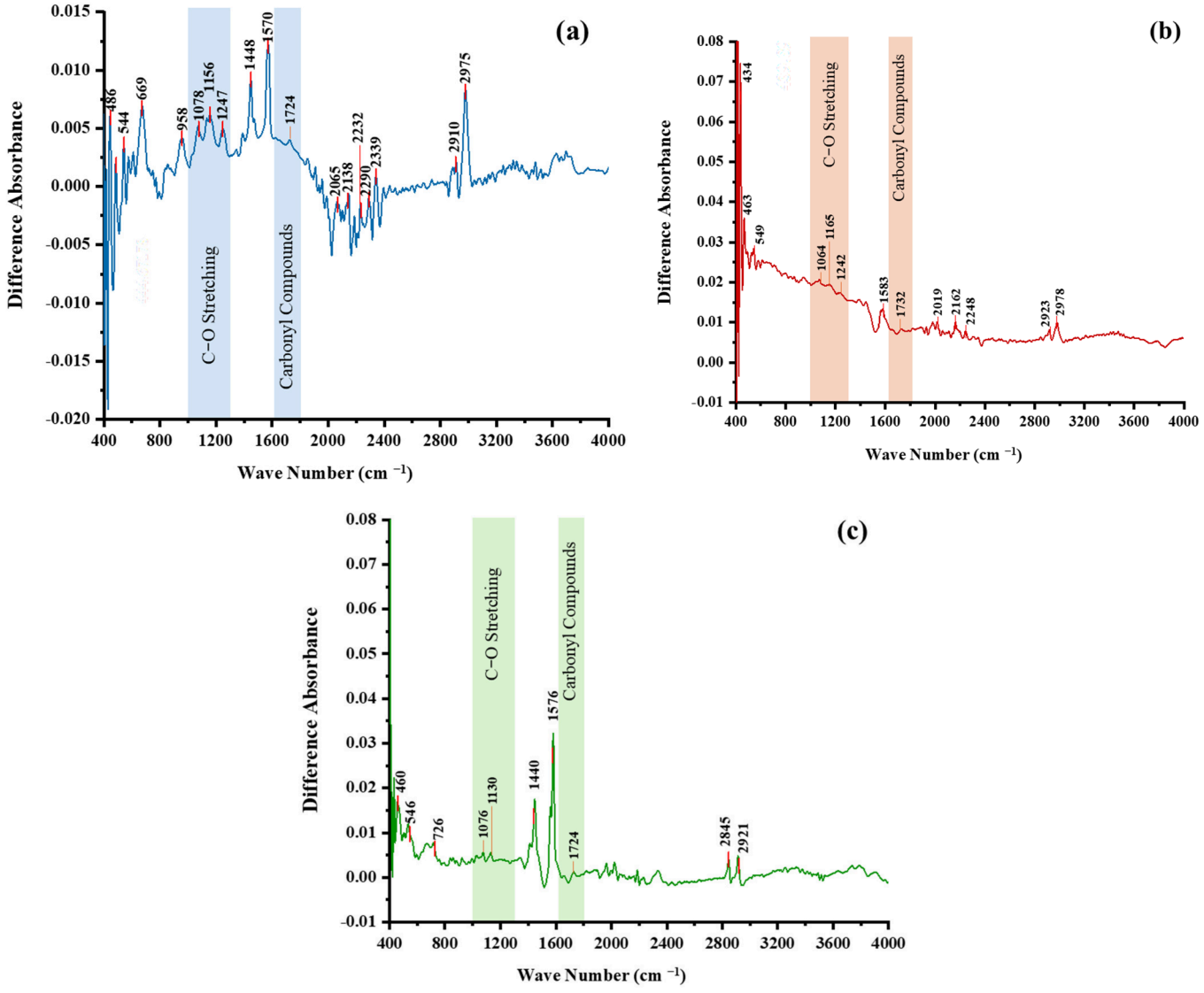

Figure 7. Difference ATR-FTIR spectra (used grease-fresh grease) obtained under no-current conditions for (**a**) base grease, (**b**) commercial grease, and (**c**) hBN grease. The shaded regions of 1800–1660 cm^{-1} and 1300–1000 cm^{-1} indicate oxidation-related carbonyl (C=O) and oxygen-containing C–O functional groups, respectively.

Under electrified conditions, the degradation behaviors of the greases were further assessed using difference ATR-FTIR spectra obtained by subtracting the spectra of fresh grease from those of the tested grease (Figure 8). The difference spectra revealed measurable

chemical alterations under electrified conditions. The positive absorbance bands indicate an increase relative to the fresh grease spectrum and may be associated with chemical changes during testing.

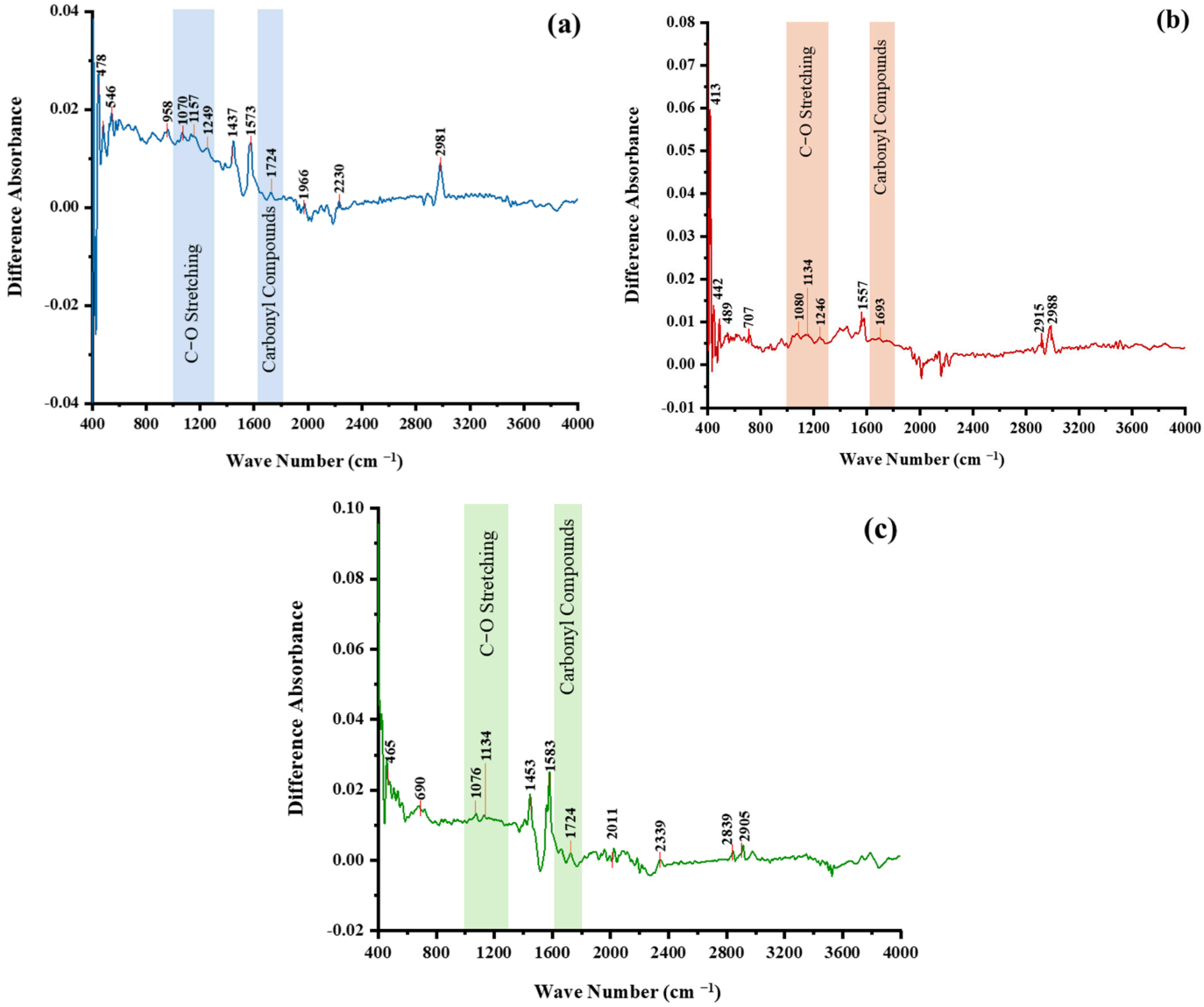

Figure 8. Difference ATR-FTIR spectra (used grease−fresh grease) obtained under electrified conditions for (**a**) base grease, (**b**) commercial grease, and (**c**) hBN grease. The shaded regions of 1800–1660 cm^{-1} and 1300–1000 cm^{-1} indicate oxidation-related carbonyl (C=O) and oxygen-containing C–O functional groups, respectively.

The base grease (Figure 8a) exhibited relatively small spectral deviations, suggesting good resistance to electrically induced chemical alteration. In contrast, the commercial grease showed larger absorbance variations than the base grease, suggesting greater chemical alteration during testing (Figure 8b). The hBN grease (Figure 8c) also exhibited noticeable spectral variations, indicating greater chemical alteration compared with the base grease. The higher magnitude of the absorbance changes observed for the commercial grease and hBN grease suggests that the electrical current promoted greater chemical alteration in these formulations. Under electrified conditions, spectral changes were also observed in the oxidation-sensitive regions of 1800–1660 cm^{-1} and 1300–1000 cm^{-1}, as highlighted in Figure 8. These regions are commonly associated with the formation of carbonyl-containing oxidation products and oxygenated compounds containing C–O link-

ages, such as alcohols, ethers, and peroxides. The commercial grease and hBN grease exhibited more pronounced absorbance changes within these regions than the base grease, suggesting a greater degree of lubricant oxidation and degradation during electrically stressed operation. However, owing to the qualitative nature of the ATR-FTIR analysis, these spectral changes should be interpreted as indicative of oxidation-related chemical transformations rather than definitive identification of specific degradation products. Nevertheless, the greater spectral changes observed under electrified conditions compared with non-electrified conditions suggest that the presence of electric current may accelerate lubricant degradation through oxidation-related processes.

Overall, the ATR-FTIR spectra indicate that the base grease exhibited superior chemical stability under both electrified and non-electrified conditions, whereas the commercial and hBN greases experienced comparatively greater chemical alteration. Although the ATR-FTIR analysis provides only qualitative evidence, the observed spectral variations are consistent with the wear debris, vibration, and surface damage results obtained in this study. The absence of strong carbonyl- or peroxide-related bands suggests that oxidation, if present, remained limited under the investigated test conditions. Since ATR-FTIR primarily identifies major chemical changes, additional characterization techniques, such as transmission FTIR, Raman spectroscopy, and X-ray photoelectron spectroscopy (XPS), may provide deeper insight into the degradation chemistry occurring under electrified tribological conditions.

3.4. Analyzing Surface Damage of Bearing Raceways During Tribo-Testing

To understand the microstructural and surface damage, the bearing raceways were analyzed using an optical microscope. Figure 9 indicates the surface damage of the bearing raceways running under the no electric current condition. Surface features resembling micro-pitting and ridge formation were observed on the raceways after the tribo-test for all greases.

Further examination of the damage to the bearing raceways through a microstructural analysis revealed the presence of surface regions morphologically similar to those of white etching areas (WEAs) reported in the literature. Previous studies have reported that hydrogen generated during electrically induced lubricant degradation may penetrate bearing steel and contribute to the formation of hydrogen-induced WEAs [49,50]. Such mechanisms have been associated with surface deterioration, crack initiation, and premature bearing failure. As shown in Figure 10, a distinct difference in microstructure was observed between the bearings lubricated with base grease and those with commercial grease under identical magnification. The damaged regions exhibited features morphologically similar to those of white etching areas (WEAs) reported in the literature. The passage of electric current through the bearings caused significant microstructural alterations. Notably, the bearings lubricated with CG and hBN grease exhibited more severe microstructural degradation compared to the one with base grease. An untested bearing raceway exhibited an average Rockwell hardness of 80 $\pm$ 1.25 HRC, while the hardness of the WEAs on the bearing raceways showed values of 81.2 $\pm$ 0.5 HRC for the base grease, 84.6 $\pm$ 0.4 HRC for the commercial grease, and 87.5 $\pm$ 0.3 HRC for the hBN grease. This increase in hardness may be associated with microstructural transformations (even formation of carbides) induced by localized thermal and electrical effects during current passage, as reported in previous studies [51,52].

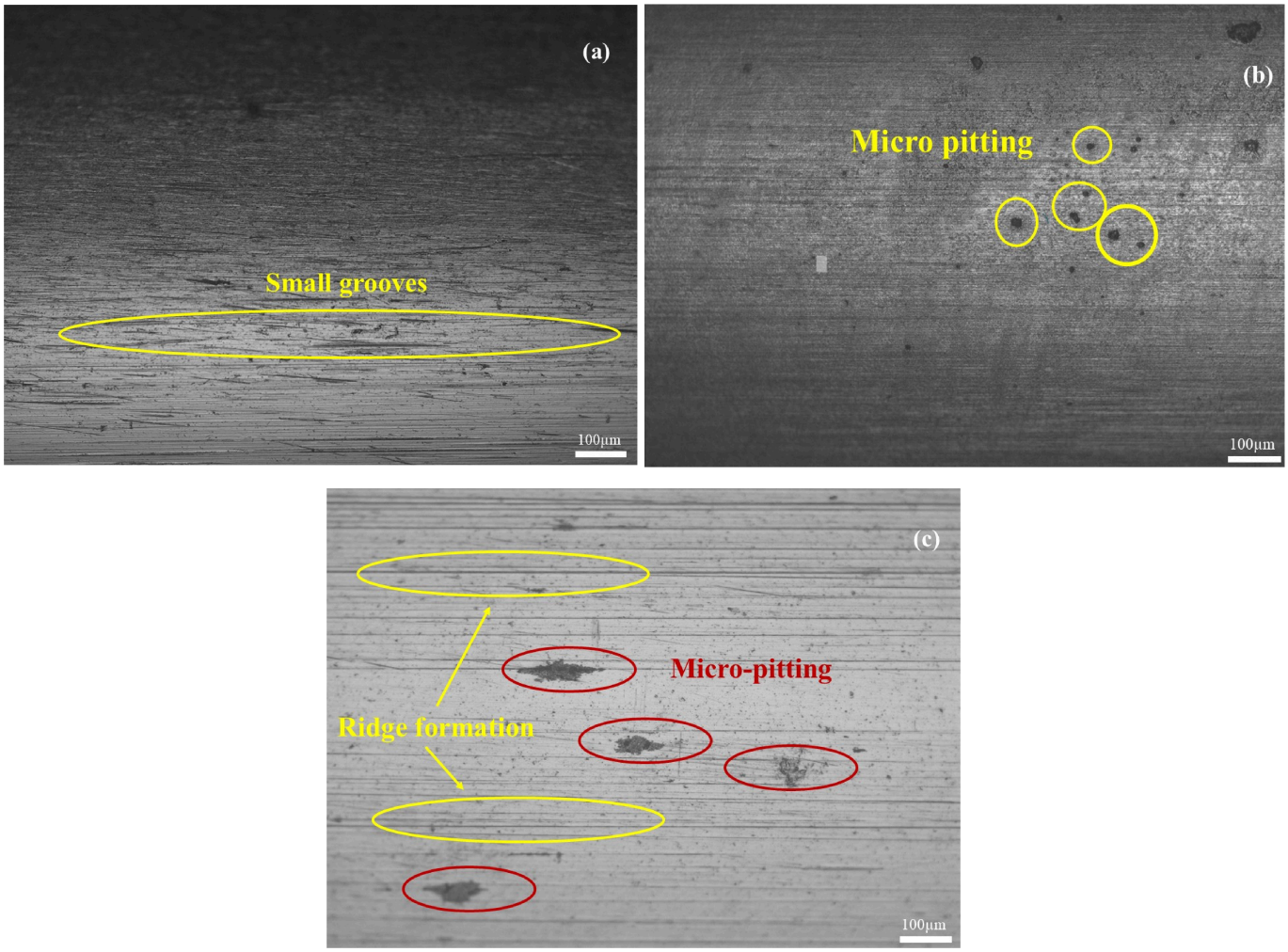

Figure 9. Surface damage observed on the bearing raceways under no-current conditions: (**a**) base grease, (**b**) commercial grease sample, and (**c**) hBN grease.

Table 7 shows the iron (Fe) content in the greases after the tribo-test. It can be seen that the Fe content in all the greases under no-current conditions was nearly the same, indicating that all the grease samples exhibited similar tribological behavior under no-current conditions (Fe content was 219 ppm for the base grease, 226 ppm for the commercial grease, and 233 ppm for the hBN grease). However, under electrified conditions, the CG and hBN greases exhibited a significantly higher rate of material removal. In the case of the base grease, the Fe concentration was found to be 231 ppm, indicating a relatively stable lubricating film, which thus protected the contact surfaces against severe wear even under electrical influence [53,54]. On the other hand, the commercial grease and hBN grease exhibited a higher Fe content of 539 ppm and 556 ppm, indicating severe wear of the bearing surfaces and extensive material removal.

Table 7. Iron content in grease after tribo-test.

Passage of Current	Grease	Unit	Fe Content
No current	Base grease	ppm	219
No current	Commercial grease	ppm	226
No current	hBN grease	ppm	233
With current	Base grease	ppm	231
With current	Commercial grease	ppm	539
With current	hBN grease	ppm	556

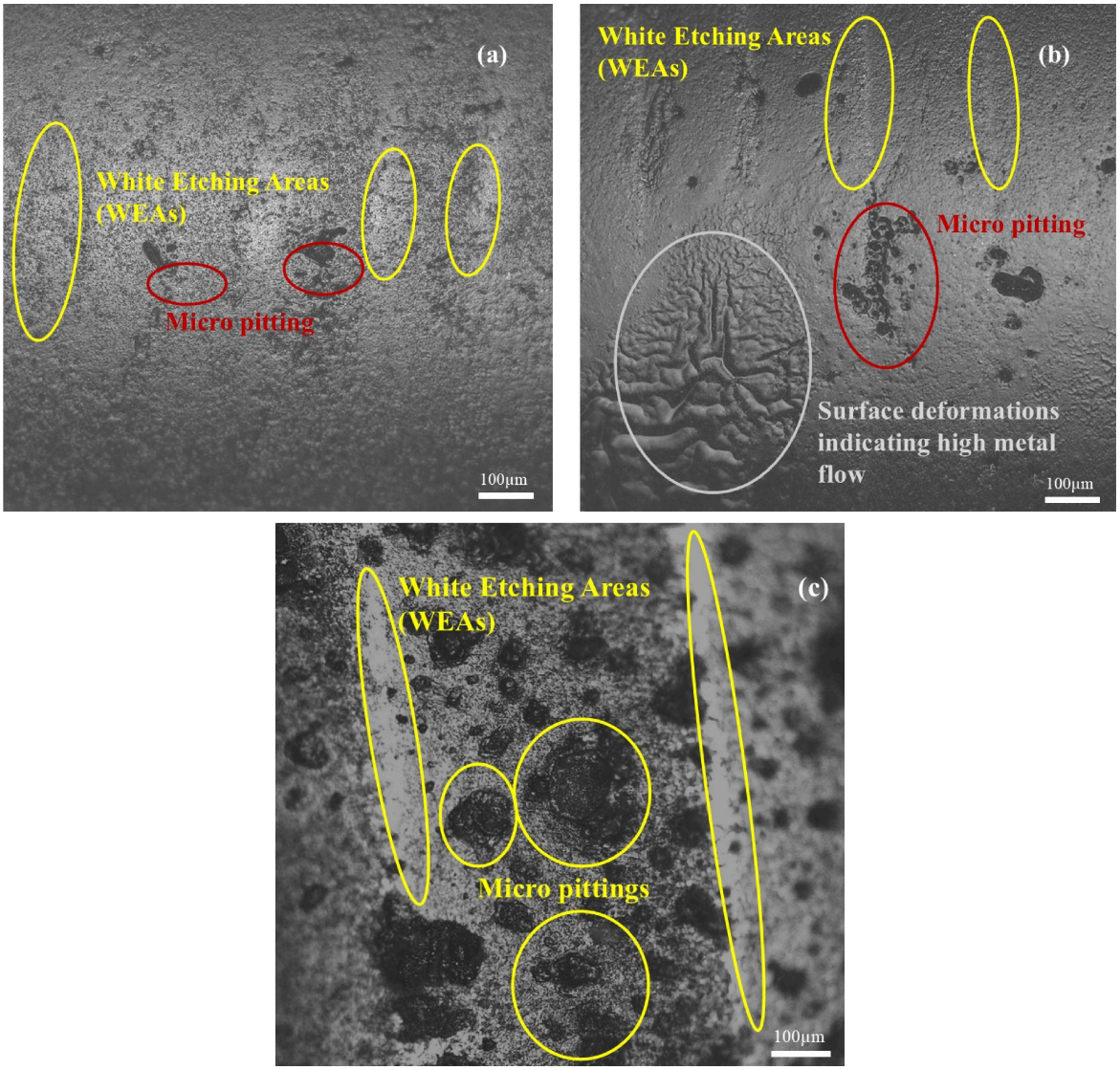

Figure 10. Formation of white etched areas (WEAs) and other surface damages on (**a**) base grease, (**b**) commercial grease, and (**c**) hBN grease.

One of the key factors influencing this behavior is the viscosity of the base oil. Although higher viscosity typically promotes the formation of a thicker lubricant film, under electrified conditions, this can be detrimental. A thicker lubricant film may impede the dissipation of electrical charges, leading to localized electrical discharges at surface asperities. These discharges generate localized heating and micro-melting at the contact interface, thereby accelerating wear and increasing Fe debris generation [54]. Furthermore, the combined effect of asperity interactions and electrical discharges promotes micro-pitting and progressive material removal from the bearing raceways. The generated wear debris becomes entrained in the lubricant and acts as abrasive particles, further exacerbating surface damage. As debris accumulation increases, the lubrication regime deteriorates, resulting in elevated friction and vibration levels. Overall, the results demonstrate that the lubricant properties, particularly the base oil viscosity, along with asperity interactions and wear debris formation, play a critical role in determining the tribological performance under electrified conditions.

3.5. Limitations of hBN as a Nano-Additive Under Electrified Conditions

One possible explanation for the inferior performance is the agglomeration of hBN nanoparticles under operating conditions [55]. Although hBN nanoparticles possess excellent solid lubrication properties, high thermal conductivity, and high dielectric strength [56], these nanoparticles exhibit a strong tendency to agglomerate due to their high surface energy and strong van der Waals forces [57]. Despite employing ultrasonication, high-shear mechanical mixing, and three-roll milling during grease preparation, the nano hBN particles likely formed micron-sized clusters rather than remaining well-dispersed primary nanoparticles [58]. Once agglomerated, these hBN clusters acted as abrasive particles rather than protective nano-spacers, promoting three-body abrasion among the rolling elements, cages, and raceways [59]. Instead of reducing friction and wear through rolling or sliding mechanisms at the contact interface, the agglomerates became embedded in softer bearing surfaces or trapped between the tribo-pairs, generating additional wear debris and accelerating surface damage [60]. This is consistent with the observed increase in iron (Fe) particles in the grease after testing (Table 7). The present study did not include a direct characterization of nanoparticle dispersion or agglomeration within the grease matrix before or after tribological testing. Although extensive dispersion procedures, including probe sonication, high-shear mixing, and three-roll milling, were employed during grease preparation, quantitative assessment of agglomerate size and distribution was not performed. Therefore, the potential contribution of nanoparticle agglomeration to the observed deterioration in the tribological and electrical performance is discussed as a plausible mechanism based on the previously reported literature rather than as direct experimental evidence obtained in the present study. Future investigations incorporating SEM-based dispersion analysis, particle size distribution measurements, and post-test microstructural characterization will be undertaken to establish a direct correlation between nanoparticle agglomeration and grease performance under electrified operating conditions.

Furthermore, the inherently insulating nature of hBN nanoparticles proved detrimental under alternating electric current conditions [61]. As a wide-bandgap electrical insulator with a high dielectric strength (typically 30–40 kV/mm) [62], hBN nanoparticles tend to block current flow rather than facilitate its controlled dissipation. In a dynamic bearing environment characterized by fluctuating contact gaps, variable lubricant film thickness, and intermittent asperity interactions, this insulating behavior promotes localized charge accumulation across tribo-pairs [63]. Under continuous operation with alternating currents ranging from 6 A to 10 A, the dispersed hBN nanoparticles effectively behaved as microscopic capacitors, storing electrical charge instead of conducting it [64]. When the accumulated charge exceeded the dielectric breakdown threshold of the lubricant film, sporadic high-energy electrical discharge events occurred instead of uniform current dissipation. These discharge events, similar to electrostatic discharge (ESD), led to localized melting, micro-welding, crater formation, and tearing of bearing surfaces [65]. The resulting rapid heating and cooling produced hard, brittle microstructures, explaining the formation of white etching areas (WEAs), micro-pitting, fluting marks, and spot welds observed on the bearing raceways lubricated with hBN grease. In contrast, the BG, with its moderate electrical conductivity derived from the base oil, enabled more uniform and continuous current dissipation, thus reducing the frequency and severity of electrical discharge damage. Essentially, the BG acted as a more stable dielectric medium, allowing for controlled current flow rather than promoting catastrophic charge buildup and breakdown. Additionally, the instability of hBN nanoparticle dispersion under the combined mechanical, thermal, and electrochemical stresses further contributed to its poor performance. Under the harsh test conditions (6–10 A current), the grease experienced intense shear forces, significant temperature rise due to frictional and Joule heating, and

electrochemical degradation. These conditions likely promoted further agglomeration, sedimentation, or phase separation of hBN nanoparticles over the 12 h test duration. As a result, the distribution of nanoparticles became highly non-uniform, with certain regions experiencing excessive agglomeration while others received little-to-no protection. The regions with high concentrations of agglomerated hBN nanoparticles suffered from accelerated abrasive wear and charge accumulation, while the regions deficient in nanoparticles reverted to the base grease's performance, compounded by degradation of the thickener structure [66]. The FTIR analysis supports this observation, showing significant chemical changes in both the commercial grease and hBN grease under electrified and non-electrified conditions, with a clear separation between the pre- and post-test spectra. In contrast, the BG exhibited minimal chemical changes, with largely overlapping FTIR curves, indicating superior chemical stability. Moreover, the elevated iron content detected in the post-test hBN grease confirms substantial wear debris generation, which further accelerated degradation through a self-perpetuating cycle of wear and contamination.

In summary,, while hBN nanoparticles possess intrinsically beneficial properties as a nano-additive, practical challenges under realistic tribological and electrified conditions significantly limit their effectiveness. These findings emphasize that nano-additive selection for electrified bearing applications must consider not only the intrinsic material properties but also compatibility with the grease matrix and stability under combined mechanical, thermal, and electrical stresses.

4. Conclusions

This work investigated the degradation of the bearing surface in the presence of hBN-enhanced lithium grease and commercial grease under varying electric current, load, and speed conditions, using a full-bearing test rig with a Taguchi L9 orthogonal experimental design. The present findings highlight the important distinction between conventional and electrified lubrication. While hBN nanoparticles have been shown to improve wear resistance in mechanically loaded contacts, their effectiveness under electrified conditions appears limited. This suggests that additive selection for electric vehicle bearing greases should consider not only tribological performance but also tribo-electrical interactions, dielectric behavior, and electrical discharge resistance.

The key conclusions derived from the work are as follows:

i The choice of lubricant is critical to protect bearings from failure due to the passage of electric current. In this work, the base grease performed significantly better than the commercial grease and hBN grease.

ii The results indicate that during the tribo-test under electrified conditions, the base grease without any additives maintained a more stable lubricating film compared to the commercial grease and optimized hBN grease.

iii The vibrations of the bearing with base grease (238.2 $\pm$ 27.83 mV) were approximately 7% less than the vibrations recorded during the test with commercial grease (337.79 $\pm$ 1.27 mV), indicating a more stable lubricating film was formed by the base grease.

iv The addition of hBN nanoparticles did not yield the expected improvement in tribological performance under electrified conditions. The inferior performance of hBN grease is attributed to nanoparticle agglomeration; poor dispersion stability under combined mechanical, thermal, and electrical stresses; and charge accumulation due to the insulating nature of hBN, which led to sporadic high-energy electrical discharge events rather than continuous current dissipation. The vibrations generated in the bearings under electrified conditions using the hBN grease (optimized) (349.4 $\pm$ 16.7 mV) were 31% higher than those using the base grease (238.2 $\pm$ 27.83 mV).

v The formation of white etching areas (WEAs), micro-pitting, weld spots, plastic deformations, and fluting marks were identified as the primary failure mechanisms from the optical microscopic images.

vi The difference ATR-FTIR spectra revealed that the base grease underwent the least chemical alteration under both electrified and non-electrified conditions, indicating its superior chemical stability. In contrast, the commercial grease and hBN grease exhibited larger absorbance variations, suggesting greater susceptibility to tribologically and electrically induced chemical changes.

vii The iron content in the grease after the tribo-test was significantly higher in the commercial grease and hBN grease compared to the base grease, confirming that substantial wear debris was generated from the bearing surfaces lubricated with the commercial grease and hBN grease. This wear debris further contaminated the lubricant and accelerated the degradation process through a self-perpetuating cycle of wear and contamination.

It should be noted that the commercial grease and the laboratory-formulated greases differed not only in the presence or absence of hBN nanoparticles but also in their overall additive chemistries. The ICP-OES analysis revealed the presence of sulfur, phosphorus, zinc, and calcium in both the commercial and formulated greases, although their concentrations varied considerably among the formulations. In addition, the hBN-containing greases exhibited substantially higher boron concentrations due to the incorporation of hBN nanoparticles. Therefore, the superior performance of the base grease observed in the present study cannot be attributed solely to the absence of hBN nanoparticles. Differences in the additive chemistries, additive concentrations, thickener–additive interactions, and electrically induced degradation mechanisms may have also contributed to the observed behavior. Further studies involving the controlled incorporation of conventional EP/AW additives together with hBN nanoparticles are required to distinguish the individual and synergistic effects of additive chemistry and hBN nanoparticles under electrified operating conditions.

Though the present work exhibits the limitations of hBN nanoparticles as a nano-additive under electrified conditions using a constant speed of 1200 rpm and varying currents (6 A–10 A) and loads (100 N–300 N), future work is planned to investigate the performance of other nano-additives with better dispersion stability, such as surface-modified nanoparticles or a hybrid nano-additive system. Additionally, longer-duration tests and advanced dispersion techniques, such as functionalization or the use of dispersants, will be explored to improve nanoparticle stability. The differences in additive chemistry, elemental composition, and additive concentrations among the grease formulations may influence the direct comparability of their tribological and electrical behavior. Future investigations should focus on systematically incorporating hBN nanoparticles into formulations containing controlled amounts of conventional AW and EP additives to distinguish the individual and synergistic effects of nanoparticle additives and additive chemistry under electrified operating conditions. The present work will be highly beneficial in understanding the practical limitations of nano-additives in grease formulations under electrified conditions, thus helping lubricant manufacturers to develop high-performance lubricants with careful consideration of dispersion stability and agglomeration prevention. A limitation of the present study is that each experimental condition was repeated twice due to the limited availability of the formulated grease samples. Although consistent trends were observed and supported by the statistical analysis, future work with additional replicates will further improve the statistical robustness of the findings.

Supplementary Materials: The following supporting information can be downloaded at: https://www.mdpi.com/article/10.3390/technologies14070389/s1, Figure S1: Main effects plot for means for current, load and %hBN, Figure S2. Main effects plot for means for current, load and %hBN, Table S1: Response tables for Signal to Noise Ration and Means.

Author Contributions: S.B.: Conceptualization, formal analysis, investigation, methodology, project administration, supervision, validation, and writing—review and editing. B.L.M.R.: Data curation, investigation, writing—original draft preparation, and writing—review and editing. V.P.: Methodology, project administration, supervision, validation, and writing—review and editing. W.W.F.C.: Methodology, project administration, and writing—review and editing. All authors have read and agreed to the published version of the manuscript.

Funding: This research received no external funding.

Institutional Review Board Statement: Not applicable.

Informed Consent Statement: Not applicable.

Data Availability Statement: Data will be made available on reasonable.

Conflicts of Interest: The authors declare no conflicts of interest.

References

1. Kempton, W.; Letendre, S.E. Electric vehicles as a new power source for electric utilities. *Transp. Res. Part D Transp. Environ.* **1997**, *2*, 157–175. [CrossRef]
2. Sun, X.; Li, Z.; Wang, X.; Li, C. Technology Development of electric vehicles. *Energies* **2020**, *13*, 90. [CrossRef]
3. Shah, R.; Gashi, B.; Rosenkranz, A. Latest developments in designing advanced lubricants and greases for electric vehicles—An overview. *Lubr. Sci.* **2022**, *34*, 515–526. [CrossRef]
4. Shah, R.; Tung, S.; Chen, R.; Miller, R. Grease Performance Requirements and Future Perspectives for Electric and Hybrid Vehicle Applications. *Lubricants* **2021**, *9*, 40. [CrossRef]
5. Salmeron, G.C.; Leckner, J.; Schwack, F.; Westbroek, R.; Glavatskih, S. Grease for electric vehicle motors: Thickener effect and energy saving potential. *Tribol. Int.* **2022**, *167*, 107400. [CrossRef]
6. Udaeta, M.; Chaud, C.A.; Gimenes, A.L.V.; Galvao, L.C.R. Electric Vehicles Analysis inside Electric Mobility Looking for Energy Efficient and Sustainable Metropolis. *Open J. Energy Effic.* **2015**, *4*, 1–14. [CrossRef]
7. Mei, J.; Zuo, Y.; Lee, C.H.T.; Kirtley, J. Modelling and Optimizing Method for Axial Flux, Induction Motor of Electric Vehicles. *IEEE Trans. Veh. Technol.* **2020**, *69*, 5236–5247. [CrossRef]
8. Cano, Z.P.; Banham, D.; Ye, S.; Hartenbach, A.; Lu, J.; Fowler, M. Batteries and fuel cells for emerging electric vehicle markets. *Nat. Energy* **2018**, *3*, 279–289. [CrossRef]
9. Martinez, M.; Hu, X.; Cao, D.; Velenis, E.; Gao, B.; Wellers, M. Energy management in plug-in hybrid electric vehicles: Recent progress and a connected vehicles perspective. *IEEE Trans. Veh. Technol.* **2017**, *66*, 4534–4549. [CrossRef]
10. Cen, H.; Lugt, P.M.; Morales-Espejel, G. On the film thickness of grease-lubricated contacts at low speeds. *Tribol. Trans.* **2014**, *57*, 668–678. [CrossRef]
11. Vengudusamy, B.; Claus, E.; Reiner, S. On the film forming and friction behaviour of greases in rolling/sliding contacts. *Tribol. Int.* **2019**, *129*, 323–337. [CrossRef]
12. Yilmaz, M.; Lohner, T.; Michaelis, K.; Stahl, K. Bearing power losses with water-containing gear fluids. *Lubricants* **2020**, *8*, 5. [CrossRef]
13. De Gaetano, D.; Zhu, W.; Sun, X.; Chen, X.; Griffo, A.; Jewell, G.W. Experimental Ball Bearing Impedance Analysis Under Different Speed and Electrical Conditions. *IEEE Trans. Dielectr. Electr. Insul.* **2023**, *30*, 1312–1321. [CrossRef]
14. Graf, S.; Capan, R.; Koch, O.; Sauer, B. Electrically induced damage of rolling bearings due to parasitic converter currents in electrical drive trains. In *Commercial Vehicle Technology 2022*; ICVTS 2022; Proceedings; Berns, K., Dressler, K., Kalmar, R., Stephan, N., Teutsch, R., Thul, M., Eds.; Springer Vieweg: Wiesbaden, Germany, 2022. [CrossRef]
15. Ma, J.; Xue, Y.; Han, Q.; Li, X.; Yu, C. Motor Bearing Damage Induced by Bearing Current: A Review. *Machines* **2022**, *10*, 1167. [CrossRef]
16. Li, Z.; Guo, F.; Jing, Z.; Li, B.; Zhang, L.; Wang, X. Study on Electric Erosion in Grease Lubrication Using Optical Interference. *Tribol. Int.* **2024**, *195*, 109596. [CrossRef]

17. Abu Saad, S.; Elmahjubi, A. Nanotechnology: Concepts, Importance and the Current State of Scientific Research. In *Proceedings of the Conference on Engineering Sciences and Technology (CEST), Libya, North Africa, 25–27 September 2018*; AIJR Books: Utraula, India, 2018; Volume 4, pp. 555–561. [CrossRef]
18. Deepika. Nanotechnology Implications for High Performance Lubricants. *SN Appl. Sci.* **2020**, *2*, 1128. [CrossRef]
19. Fei, Y.W.; Ruan, S.J.; Ma, J.; Guo, F. Study on Thermal Oxidation and Viscosity Degradation for Synthetic Aviation Lubricant Fluids. *IOP Conf. Ser. Mater. Sci. Eng.* **2020**, *729*, 012072. [CrossRef]
20. Tajedini, M.; Bahrami, R.; Azhdari, R.; Sue, H.J.; Liang, H. Influence of electric current on tribological performance of grease lubricated steels. *Tribol. Int.* **2024**, *200*, 110121. [CrossRef]
21. Qu, J.; Bansal, D.G.; Yu, B.; Howe, J.Y.; Luo, H.; Dai, S.; Li, H.; Blau, P.J.; Bunting, B.G.; Mordukhovich, G.; et al. Antiwear performance and mechanism of an oil-miscible ionic liquid as a lubricant additive. *ACS Appl. Mater. Interfaces* **2012**, *4*, 997–1002. [CrossRef] [PubMed]
22. Ge, X.Y.; Xia, Y.Q.; Feng, X. Influence of carbon nanotubes on conductive capacity and tribological characteristics of poly (ethylene glycol-ran-propylene glycol) mono butyl ether as base oil of grease. *Trans. ASME-J. Tribol.* **2015**, *138*, 011801. [CrossRef]
23. Hassan, A.M.; Shahba, R.M.A.; Youssif, M.A.; Mazrouaa, A.M.; Youssif, M.A.E. Preparation of some dielectric greases from different types of polymers. *J. Appl. Polym. Sci.* **2011**, *119*, 1026–1033.
24. Pojanavaraphan, T.; Schiraldi, D.A.; Magaraphan, R. Mechanical, rheological, and swelling behaviour of natural rubber/montmorillonite aerogels prepared by freeze-drying. *Appl. Clay Sci.* **2010**, *50*, 271–279. [CrossRef]
25. Li, Z.; Guo, F.; Jing, Z.; Li, B.; Zhang, L.; Wang, X. Study on Grease Lubrication and Electric Erosion Characteristics in AC Electric Fields. *Lubricants* **2024**, *12*, 79. [CrossRef]
26. Urunuela, L.; Fernandez-Diaz, B.; Pagano, F.; Lopez Ortega, A.; Pinedo, B.; Bayon, B. Broad review of White Etching Crack failure in wind turbine gearbox bearings, Main factors and experimental investigations. *Int. J. Fatigue* **2021**, *145*, 106091. [CrossRef]
27. Esmaeili, K.; Wang, L.; Harvey, T.J.; White, N.M.; Holweger, W. Electrical discharges in oil-lubricated rolling contacts and their detection using electrostatic sensing technique. *Sensors* **2022**, *22*, 392. [CrossRef] [PubMed]
28. Gonda, A.; Capan, R.; Bechev, D.; Sauer, B. The influence of lubricant conductivity on bearing currents in the case of rolling bearing greases. *Lubricants* **2019**, *7*, 108. [CrossRef]
29. Turnbull, R.; Rahmani, R.; Paul, S.; Rahnejat, H. Electrotribodynamics of ball bearings in electrical machines. *Tribol. Int.* **2023**, *188*, 108817. [CrossRef]
30. Bleger, A.; Leighton, M.; Morris, N. Automotive e-motor bearing electrical discharge phenomena: An experimental and numerical investigation. *Tribol. Int.* **2024**, *191*, 109140. [CrossRef]
31. Zhang, P.L.; Wang, G.; Zhao, Y.; Wu, J.; Xia, H.; Xia, Y.Q. Study of conductive and friction properties of grease containing carbon black additive. *Adv. Mater. Res.* **2015**, *1120*, 586–589. [CrossRef]
32. Martin, G.; Becker, F.M.; Kirchner, E. A novel method for diagnosing rolling bearing surface damage by electric impedance analysis. *Mech. Syst. Signal Process.* **2022**, *170*, 107503. [CrossRef]
33. Randall, R.B. *Vibration-Based Condition Monitoring: Industrial, Aerospace, and Automotive Applications*; John Wiley & Sons: Chichester, UK, 2011. [CrossRef]
34. Van Hecke, B.; Yoon, J.; He, D. Low speed bearing fault diagnosis using acoustic emission sensors. *Appl. Acoust.* **2016**, *105*, 35–44. [CrossRef]
35. Schirra, T.; Martin, G.; Puchtler, S.; Kirchner, E. Electric impedance of rolling bearings—Consideration of unloaded rolling elements. *Tribol. Int.* **2021**, *158*, 106927. [CrossRef]
36. Beroual, A.; Khaled, U.; Noah, P.; Sitorus, H. Comparative Study of Breakdown Voltage of Mineral, Synthetic and Natural Oils and Based Mineral Oil Mixtures under AC and DC Voltages. *Energies* **2017**, *10*, 511. [CrossRef]
37. El-Adly, R.A.; Turky, G.M. Comparative study between prepared electrical grease and the imported one. *Egypt. J. Pet.* **2018**, *27*, 209–213. [CrossRef]
38. Cheng, Y.; Bu, Y.; Guan, P.; Yang, Y.; Qing, J. Tribological properties of hexagonal boron nitride nanoparticles as a lubricating grease additive. *Lubr. Sci.* **2023**, *35*, 449–458. [CrossRef]
39. Bhaumik, S.; Yunus, M.; Jothikumar, S.; Hareesh, G.; Paleu, V.; Sharma, A.K.; Mavani, S. Exploring the Failures of Deep Groove Ball Bearings Under Alternating Electric Current in the Presence of Commercial Lithium Grease. *Technologies* **2025**, *13*, 275. [CrossRef]
40. Ono, A. Revision of the Standard Method (JIS G 1253) for Spark Discharge Atomic Emission Spectrometry of Iron and Steel. *Tetsu-Hagané* **1995**, *81*, 869–875. [CrossRef]
41. Kumar, N.; Saini, V.; Bijwe, J. Performance properties of lithium greases with PTFE particles as additive: Controlling parameter-size or shape. *Tribol. Int.* **2020**, *148*, 106302. [CrossRef]
42. Li, J.; Lin, N.; Du, C.; Ge, Y.; Amann, T.; Feng, H. Tribological behaviour of cellulose nanocrystal as an eco-friendly additive in lithium-based greases. *Carbohydr. Polym.* **2022**, *290*, 119478. [CrossRef] [PubMed]

43. Bai, P.; Li, S.; Tao, D.; Jia, W.; Meng, Y.; Tian, Y. Tribological properties of liquid-metal Galinstan as novel additive in lithium grease. *Tribol. Int.* **2018**, *128*, 181–189. [CrossRef]
44. Gangwani, P.; Gupta, M.K.; Bijwe, J. Synergism between particles of PTFE and hBN to enhance the performance of oils. *Wear* **2017**, *376–377*, 762–770. [CrossRef]
45. Mikami, H.; Kawamura, T. Influence of Electrical Current on Bearing Flaking Life. In Proceedings of the SAE World Congress & Exhibition, Detroit, MI, USA, 16 April 2007. [CrossRef]
46. Wu, N.; Zong, Z.M.; Fei, Y.W.; Ma, J. Studies on Thermal Oxidation Stability of Aviation Lubricating Oils. *MATEC Web Conf.* **2017**, *114*, 02002. [CrossRef]
47. Suzumura, J. Prevention of Electrical Pitting on Rolling Bearings by Electrically Conductive Grease. *Q. Rep. RTRI* **2016**, *57*, 42–47. [CrossRef] [PubMed]
48. Sanchez, L.J.; Hager, C.H.; Evans, R.D. Rolling Element Bearing Damage in the Presence of Applied Electric Current. *Tribol. Trans.* **2024**, *67*, 602–613. [CrossRef]
49. Zhang, X.; Huang, X.; Li, J.; Tang, Z.; Wang, J. Thermal oxidation of aviation lubricating oil: Mechanism, influencing factors, evaluation methods, and antioxidants. *J. Appl. Polym. Sci.* **2024**, *141*, e3114. [CrossRef]
50. Sreeraj, K.; Ramkumar, P. Replication of white etching area evolution using novel modified dynamic load pin-on-disc tribometer on bearing steel. *Tribol. Int.* **2018**, *126*, 336–343. [CrossRef]
51. Bai, B.; Davis, L.; Ramkumar, P. Electrical current effects on white etching areas formation in bearing steel under dynamic loading. *Wear* **2025**, *570*, 205977. [CrossRef]
52. Zhang, D.; Zheng, H.; Hou, T.; Hu, F.; Zheng, P.; Wu, K. Hardness increases due to (Fe, Cr)2C carbide precipitated during natural aging in high chromium cast iron. *J. Mater. Res. Technol.* **2023**, *209*, 111766. [CrossRef]
53. Xie, G.X.; Luo, J.B.; Liu, S.H.; Guo, D.; Li, G.; Zhang, C.H. Effect of Liquid Properties on the Growth and Motion Characteristics of Micro-Bubbles Induced by Electric Fields in Confined Liquid Films. *J. Appl. Phys.* **2009**, *105*, 115502. [CrossRef]
54. Raadnui, S.; Kleesuwan, S. Electrical pitting wear debris analysis of grease-lubricated rolling element bearings. *Wear* **2011**, *271*, 1707–1718. [CrossRef]
55. Liu, W.; Qiao, X.; Liu, S.; Chen, P. A Review of Nanomaterials with Different Dimensions as Lubricant Additives. *Nanomaterials* **2022**, *12*, 3780. [CrossRef] [PubMed]
56. Jiang, H.; Cai, Q.; Srikanth, M.; Amrito, B.; Yuanlie, Y.; Zeng, X.; Sun, R.; Huang, S.; Chen, Y.I. Recent research advances in hexagonal boron nitride/polymer nanocomposites with isotropic thermal conductivity. *Adv. Compos. Mater.* **2024**, *1*, 144–156. [CrossRef]
57. Garcia Tobar, M.; Contreras Urgiles, R.W.; Jimenez Cordero, B.; Guillen Matute, J. Nanotechnology in Lubricants: A Systematic Review of the Use of Nanoparticles to Reduce the Friction Coefficient. *Lubricants* **2024**, *12*, 166. [CrossRef]
58. Sidh, K.N.; Jangra, D.; Hirani, H. An Experimental Investigation of the Tribological Performance and Dispersibility of 2D Nanoparticles as Oil Additives. *Lubricants* **2023**, *11*, 179. [CrossRef]
59. Zhao, B.; Zhang, Y.; F, Y.; Yu, X.; Zhang, Z.; Zhang, B. The three-body abrasive tribological characteristics of the Graphene/h-BN heterostructure film considering defects. *Tribol. Int.* **2022**, *171*, 107525. [CrossRef]
60. Dimitriadi, M.; Zinelis, S.; Zafiropoulou, M.; Silikas, N.; Eliades, G. Self-Etch Silane Primer: Reactivity and Bonding with a Lithium Disilicate Ceramic. *Materials* **2020**, *13*, 641. [CrossRef] [PubMed]
61. Sangineni, R.; Baruah, N.; Nayak, S.K. Analysis of electric field in liquid dielectric on addition of nanoparticles. *Mater. Today Proc.* **2020**, *33*, 451–456. [CrossRef]
62. Knobloch, T. The performance limits of hexagonal boron nitride as an insulator for scaled CMOS devices based on two-dimensional materials. *Nat. Electron.* **2021**, *4*, 98–108. [CrossRef]
63. Wang, X.; Wang, J.; Davies, C.; Mo, A.; Liu, S.; Ren, N. Surface asperity-enhanced micro electrical discharge in lubricated contact interfaces. *Tribol. Int.* **2025**, *209*, 110742. [CrossRef]
64. Senyk, S.; Chodkiewicz, A.; Gocman, K.; Szczęśniak, B.; Kałdoński, T. Hexagonal Nano and Micro Boron Nitride: Properties and Lubrication Applications. *Materials* **2022**, *15*, 955. [CrossRef] [PubMed]
65. Lokhande, R.; Mishra, S.; Ronanki, D.; Shakya, P.; Edachery, V.; Koottaparambil, L. Review on Tribological and Vibration Aspects in Mechanical Bearings of Electric Vehicles: Effect of Bearing Current, Shaft Voltage, and Electric Discharge Material Spalling Current. *Lubricants* **2025**, *13*, 349. [CrossRef]
66. Shekhawat, D.; Jain, A.; Vashishtha, N.; Singh, A.P.; Kumar, R. Tribological Performance Comparison of Lubricating Greases for Electric Vehicle Bearings. *Lubricants* **2025**, *13*, 108. [CrossRef]

Disclaimer/Publisher's Note: The statements, opinions and data contained in all publications are solely those of the individual author(s) and contributor(s) and not of MDPI and/or the editor(s). MDPI and/or the editor(s) disclaim responsibility for any injury to people or property resulting from any ideas, methods, instructions or products referred to in the content.